Regularized Active Shape Model for Shape Alignment

Ran He, Zhen Lei, Xiaotong Yuan, Stan Z. Li
Institute of Automation, Chinese Academy of Sciences, Beijing, China
95 Zhongguancun Donglu, Beijing 100080, China
{rhe,zlei,szli,xtyuan}@nlpr.ia.ac.cn

Abstract

Active shape model (ASM) statistically represents a shape by a set of well-defined landmark points and models object variations using principal component analysis (PCA). However, the extracted shape contour modeled by PCA is still unsmooth when the shape has a large variation compared with the mean shape. In this paper, we propose a regularized ASM (R-ASM) model for shape alignment. During training stage, we present a regularized shape subspace on which image smoothness constraint is imposed, such that the learned components to model shape variations should not only minimize reconstruction error but also obey smoothness principle. During searching stage, a coarse-to-fine parameter adjustment strategy is performed under Bayesian inference. It makes a desired shape smoother and more robust to local noise. Lastly, an inner shape is introduced to further regularize search results. Experiments on face alignment demonstrate the efficiency and effectiveness of our proposed approach.

1. Introduction

Shape analysis is an active area in computer vision. A common task of shape analysis is to recover both pose parameters and low-dimensional representation of the underlying shape from an observed image. Applications of shape analysis spread from medical image processing, face recognition, object tracking and etc. A lot of approaches have been proposed for shape analysis in the past decades. Among them, the Active Shape Model (ASM) [1, 2] is the most flexible methodology and has been deeply researched.

In order to learn a robust statistical model and retrieve a smooth object contour, many shape models have been developed to further improve ASM's performance. They mainly emphasize on two parts: (1) statistic framework to estimate the shape and pose parameters and (2) optimal features to accurately model appearance around landmarks. For parameter estimation, Zhou, Gu, and Zhang [3] propose a Bayesian tangent shape model to estimate parameters more accurately by Bayesian inference. Coughlan and Ferreira [4] introduce a Markov Random Field model to model both the local image structure and the shape prior. Liang et al. [5, 6] adopt Markov network to find an accurate shape which is regularized by the PCA based shape prior through a constrained regularization algorithm. Li and Ito [7] use AdaBoosted histogram classifiers to model local appearances and optimize shape parameters. Thomas Brox et al. [8] integrated 3D shape knowledge into a variational model for pose estimation and image segmentation. V. Blanz et al. [20] uses Bayesian method to estimate 3D shape parameter. Huang et al [12] use a nonlinear constrained Gaussian process latent variable model to represent global shape prior. For optimal features, van Ginneken et al. [9] propose a non-linear ASM with Optimal Features (OF-ASM), which allows distributions of multi-modal intensities. Federico Sukno et al. [10] further develop this non-linear appearance model, incorporating a reduced set of differential invariant features as local image descriptors. A Cascade structure containing multiple ASMs is introduced in [11] to make location of landmarks more accurate and robust. Recently, Huang et al. [12] propose an illumination robust feature to model local information of landmark points when illumination changes dramatically. However, when these methods are applied to face alignment, the searched face contours are still unsmooth and couldn't well represent large deformation.

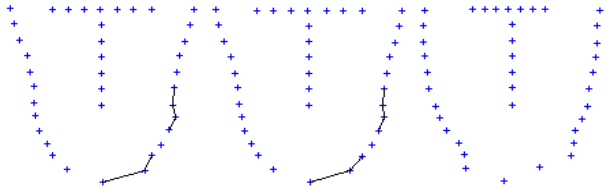

Figure 1: (a) Cheek shape reconstructed by a PCA eigenvector when the corresponding shape parameter is equal $3\sqrt{\lambda_i}$ (λ_i is the eigenvalue). (b) Cheek shape reconstructed by a RSS eigenvector when the corresponding shape parameter is equal to $3\sqrt{\lambda_i}$. (c) Cheek shape reconstructed by a PCA eigen vector corresponding to a small eigenvalue when shape parameter has a large value.

A human face contour has large deformations and is a smooth object shape. When applying deformable mode to face alignment, we find that an unsmooth boundary comes not only from local noise but also from ASM model itself.

978-1-4244-2154-1/08/$25.00 ©2008 IE

In ASM and its derivations, the principle component analysis (PCA) technique is used to model face shape deformation or to build a Gaussian shape prior. A new shape is expressed as a linear combination of the principal components learned from PCA. Here, we call these principal components as basis shapes. Because there is no a smooth constrain on these basis shapes, we couldn't ensure that a new shape expressed by these basis shapes is smooth. Fig.1 (a) shows an example shape constructed by one basis shape. It is obvious that this shape is unsmooth in some parts. Furthermore, shape parameters with large eigen value model main variation of a face and those with small eigen values describe face's local details. When the value of shape parameter is close to or larger than eigen value, the generated new shape would lose their semantic information and becomes unpredictable. Fig.1 (c) illustrates one example of this scenario. To tackle these problems, we would consider applications of smoothness constraints.

In this paper, we firstly propose a Regularized Shape Subspaces (RSS) for regularizing PCA shape subspace. The smoothness constrain is imposed on the subspace components should not only minimize the construction error but also obey the smoothness principle. Fig.1 (b) show a shape expressed by single shape basis learned by RSS. Secondly, Bayesian risk minimization theory is introduced to learn a smooth shape during a new shape search. This makes parameter estimation more robust to local noise and leads to a coarse-to-fine shape search. This parameter estimation method can also be viewed as a shape parameter regularization method. But different from isotropic noise in the tangent space [3,5,6], our method assumes that the noise comes from each landmark's inaccurate searching. Thirdly, we construct an inner shape from some landmarks that are easy to be located. The inner shape is constructed by eyes and mouth center which can be accurately detected by appearance-based method. We use the inner shape to estimate ASM's pose parameter and further regularize search results.

2. Overview of ASM

This section briefly reviews the ASM segmentation scheme. We follow the description and notation of [2]. An object is described by points, referred as landmark points. The landmark points are (manually) determined in a set of K training images. From these collections of landmark points, a point distribution model (PDM) [13] is constructed as follows. The landmark points ($x_1,\ldots,x_n$, $y_1,\ldots,y_n$) are stacked in shape vectors.

$$D_k = (x_1,..,x_n,y_1,..,y_n)^T \quad (1)$$

where T denotes the transpose, PCA is applied to the shape vectors D_k by computing the mean shape and covariance matrix:

$$\bar{x} = (1/K)\sum_{k=1}^{K} D_k \quad (2)$$

and

$$S = (K/(K-1))\sum_{k=1}^{K}(D_k-\bar{x})(D_k-\bar{x})^T \quad (3)$$

The eigenvectors of S corresponding to the N largest eigen values λ_n are retained in a matrix $F=\{F_1,..,F_N\}$. A shape can now be approximated by

$$x \approx \bar{x} + b^T F \quad (4)$$

Where b is a vector of N elements containing the shape parameters, termed by shape parameter, computed by

$$b = F^T(x-\bar{x}) \quad (5)$$

Before PCA is applied, the shapes can be aligned by translating, rotating and scaling so as to minimize the sum of squared distances between the landmark points. We can express the initial estimate x of a shape as a scaled, rotated and translated version of original shape.

$$x = M(s,\theta)[x] + t \quad (6)$$

Where $M(s,\theta)$ and t are pose parameters (See [1] for details). Procrustes analysis [14] and EM algorithm [3] are used to estimate pose parameters and align the shapes.

3. Regularized Shape Subspaces

Let $D=\{D_1,D_2,\ldots,D_k\}$ be a training set of K shape examples, where an shape sample D_k is a shape vector. An ASM method learns from the training data D and ordered set of N basis shapes $F=\{F_1,..,F_N\}$, where F_n is a vector of the same size as D_k.

The learning of basis shapes F may be done by minimizing a cost function $E(D|F)$

$$F^* = \arg\min_F E(D \mid F) \quad (7)$$

Where $E(D|F)$ is associated with some likelihood distribution $P(D|F)$. The cost function for standard PCA is the squared reconstruction error, subject to orthonormal constrains imposed on $F^{(n)}$

$$\min_F E(D \mid F) = \min_F \sum_{k=1}^{K} \| \sum_{n=1}^{N} ((F_n)^T * D_k) * F_n - D_k \|^2 \quad (8)$$

$$s.t. \quad \| F_n \| = 1 \quad \& \quad F_n^T * F_{n'} = 0, \forall n \neq n'$$

Note that $F_n(x,y)$ should be smooth shapes in the image plane. When F_n strive their best to minimize $E(D|F)$, they may overfit to the training examples D, especially when the training set is small, and the subspace model thus learned may not give good generalization to unseen shapes.

RSS learning attempts to reduce overfitting by imposing a priori constraint of smoothness. The smoothness constraint is imposed on the basis functions $F_n(x,y)$ so that $F_n(x,y)$ are smooth functions of (x,y). Let us consider the membrane type of regularizer composed of the first-order derivative terms. The smoothness term is defined as:

$$E(F) = \sum_n w_n E(F_n) \quad (9)$$

Where w_n are importance weights and

$$E(F_n) = \int_{x,y} \left[(F_n^x(x,y))^2 dx + (F_n^y(x,y))^2 dy \right] \quad (10)$$

Where F_n^x and F_n^y are the first partial derivatives of the bases functions.

In the case of shapes, (x,y) take values on a discrete grid and the point (x,y) is given an order number i. Then the first derivatives may be approximated using the first order differences: $F_n^x(x,y) = F_{nx}(i) - F_{nx}(i-1)$ and $F_n^y(x,y) = F_{ny}(i) - F_{ny}(i-1)$. $F_{nx}(i)$ and $F_{ny}(i)$ are the *ith* point's coordinates of x and y respectively. Then, the membrane type of regularizer for F_n is expressed in discrete form as:

$$E(F_n) = \sum_i [(F_{nx}(i) - F_{nx}(i-1))^2 + (F_{ny}(i) - F_{ny}(i-1))^2] \quad (11)$$

Assuming $w_1 = w_2 = \cdots = w_N = w$, we can rewrite Equ. (11) in the following matrix representation:

$$E(F) = w * trace(F^T V F) \quad (12)$$

The definition of matrix V is left to the appendix A. Unless otherwise stated, we would focus on the case when w_n are equal to w for practical implementation, which would help to reduce the number of parameters for tuning.

Then we define the cost function for RSS as a combination of Equ.(8) and Equ.(9) as follows

$$E(F \mid D) = E(D \mid F) + E(F) \quad (13)$$
$$s.t. \quad \| F_n \| = 1 \quad \& \quad F_n^T * F_{n'} = 0, \forall n \neq n'$$

Fig.1 (b) shows a shape reconstructed by RSS. It is easy to find that the border of RSS reconstructed shape is smoother than that of PCA reconstructed shape.

In RSS, the smoothness constraint of $E(F)$ is combined with the constraint of $E(D|F)$ due to data D, giving rise to balanced cost $E(F|D)$. Minimizing $E(F|D)$ leads to a result of balance between the original cost and the smoothness. Such F will be smoother functions of the spatial coordinates (x,y) than obtained by minimizing $E(D|F)$ only. In addition, the smoothness constraint used in $E(F)$ can be altered to Laplacian penalty function which is of second order derivative. The parameter w is an important factor to tune the balance of $E(D|F)$ and $E(F)$. RSS method makes energy more condense to the first several eigen values. Given a large value of w, RSS will reduce the number of eigenvectors which contain semantic variation of shapes. Hence, we suggest that value of w should be smaller than the smallest eigen value corresponding to eigen vectors.

4. Bayesian Estimation

Considering that basis shapes corresponding to larger eigen values model shape's large variation and those corresponding to smaller ones model shape's local details, we use Bayesian estimation to lead a coarse-to-fine shape parameter adjustment strategy during searching a shape.

In Bayesian estimation, a risk is minimized to obtain the optimal estimate. The Bayesian risk of estimate f^* is defined as

$$R(f^*) = \int C(f^*, f) P(f \mid d) df \quad (14)$$

where d is the observation, $C(f^*,f)$ is a cost function and $P(f|d)$ is the posterior distribution. Minimizing Equ.(14) is equivalent to maximizing the posterior probability (see [18] for details)

$$f^* = \arg\max P(f \mid d) \quad (15)$$

In ASM, a shape f is expressed by the shape parameter b. Then we want to learn an optimal parameter b^*.

$$b^* = \arg\max_{b \in B} P(b \mid d) \quad (16)$$

Assuming that the observation b is the true shape contour plus an isotropic Gaussian noise ε, we can rewrite the ASM model as

$$d = \bar{x} + b^T F + \varepsilon \quad (17)$$
$$d - \bar{x} - b^T F = \varepsilon \quad (18)$$

where shape parameter b is an n-dimensional vector distributed as multivariate Gaussian $N(0,\Lambda)$ and $\Lambda = diag(\lambda_1, ..., \lambda_N)$, and F is matrix containing the eigenvectors learned by PCA or RSS. The ε is a n-dimensional random vector which is independent with b and distributes as

$$p(\varepsilon) \sim \exp\{-\| \varepsilon \|^2 / 2(\sqrt{\rho})^2\} \quad (19)$$
$$\rho = \sum_{i=1}^{n} \alpha_i \| d_i^{old} - d_i \|^2 \quad (20)$$

where d^{old} is the shape estimated in the last iteration and d is an observed shape in the current iteration. a_i is classification confidence related to a classifier used in locating a landmark. a_i equals to 0 implies that classifier can perfectly predict shape's boundary; while a_i equals to 1 means classifier fails to predict the boundary.

Combing Equ.(18) and Equ.(19), we obtain the likelihood of model parameters:

$$P(b \mid d) = const P(d \mid b) P(b) \propto \quad (21)$$
$$\exp(-\frac{1}{2}[(d - \bar{x} - b^T F)^T (d - \bar{x} - b^T F) / \rho + b^T \Lambda^{-1} b])$$

Let $\frac{\partial}{\partial b}(\ln P(b \mid y)) = 0$, we get:

$$b_j^* = (\lambda_j / (\lambda_j + \rho)) F_j^T (d - \bar{x}) \quad (22)$$

where λ_j is the *jth* eigen value learned by PCA or RSS. Because ASM's shape parameter $b_j = F_j^T (d - \bar{x})$, it follows:

$$b_j^* = (\lambda_j / (\lambda_j + \rho)) b_j \quad (23)$$

It is clear that Equ.(23) is also a constrained regularization method to optimize the shape parameter b. In [3], ρ is set to a fixed value and represents the residual variance. And in [6], the constrained regularization is tuned by the position's probability. When using regularization method, we will find that two problems: 1) b_j^* is always smaller than b_j because ρ is larger than zero. 2) The relationship between ρ and eigen value is unknown. The parameter b_j corresponding to a smaller eigen value will receive a large punishment if ρ has a large value.

Hence, we introduce a compensating factor p_1 and a smoothing factor p_2 to lead a coarse-to-fine shape

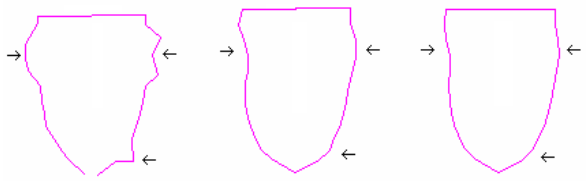

Figure 2: Shapes reconstructed from PCA and Bayesian Inference. Left shape is mean shape after desired movements; middle shape is reconstructed by PCA; right shape is reconstructed by Bayesian estimation.

parameter adjustment.

$$b_j = (p_1\lambda_j / (\lambda_j + p_2\rho))b_j \qquad (24)$$

where $1 \le p_1 \le (\lambda_{\max} + p_2\rho)/\lambda_{\max}$, $p_2 \ge 1$. The compensating factor p_1 is introduced to make shape variation along eigenvectors corresponding to large eigen values more aggressive. Moreover, because we expect a smooth shape contour and neglect details in the first several iterations, the smoothing factor p_2 is introduced to further punish shape parameter b_j. It should be noticed that ρ will become smaller and all punishment will disappear. As in Fig.2, the reconstructed shape's contour by Bayesian inference is smoother than the one by PCA in regions pointed by the black arrows. Although the PCA reconstruction can remove some noise, the reconstructed shape is still unstable when the image is noisy. Equ.(24) makes the parameter estimation more robust to local noise. We suggest that p_1 is set to $(\lambda_{\max} + p_2\rho)/\lambda_{\max}$ and p_2 are manually tuned according to experiments.

5. Inner Shape Constrain

Face detection problem has been well defined, and many efficient yet simple methods have been proposed to resolve this problem [17]. We can easily and accurately detect the coordinates of eyes and mouth by appearance-based method. How can we use these methods to improve ASM's searching result? Instead of simply giving a good initial position, we further introduce the inner shape to the ASM as a part of PDM.

For a face contour, the inner shape is composed of 13 landmarks derived from three given points: left eye center, right eye center and mouth center. We term the three points as fixed points. Five landmarks are added equidistantly between two eyes center to represent horizontal connected line. And five landmarks are inserted equidistantly in the vertical line passing the mouth center and perpendicular to the horizontal line. Those 13 landmarks are directly combined into the PDM in both training and searching.

During training phase, the coordinates of fixed points are calculated by the mean value of the coordinates of landmarks around eyes and mouth. All shapes are aligned according to two eyes centers and mouth center only. During searching phase, the initial coordinates of fixed points are automatically calculated by eye detection and mouth detection algorithm. At each iteration, the coordinates of fixed points are automatically revised by the mean value of landmarks around eyes and mouth.

6. Experiments

In this section, we test our proposed method on two experiments: cheek contour search and facial contour search. We randomly select 100 face images from the XM2VTS face database. [15] Each face is aligned by the fixed points. The average distance between two eyes is 80 pixels. Three points of the fixed shape are manually labeled in training and automatically detected in testing. The inner shape takes a shape of letter 'T' (see Fig.1). Hamarneh's ASM source code [16] is taken as the standard ASM without modification. Optimal features are

Figure 3: Comparison of different algorithms' cheek searching results: Shapes in first row are results of ASM searching; Shapes in second row are results of simple OF-ASM; Shapes in third row are results of R-ASM with OF.

Figure 4: Comparison results of ASM and our method. The first row is ASM results, and the second row is R-ASM's results.

collected from features reported in both paper [9] and [10]. The number of optimal features is reduced by sequential feature selection [19]. All points near the landmarks are classified by a linear regression to predict whether they lie in or out of a shape.

6.1. Experiments on Cheek Contour

A difficult task to directly search a cheek contour is presented to validate our method. A total of 25 cheek landmarks are labeled manually on each image. The PCA thresholds are set to 99% for every ASMs. The inner shape is composed of points between two eyes and mouth. During search, the inner shape is fixed to the initial value.

Looking at Fig.3, the first two rows are the searching results of ASM and OF-ASM. It is clear that some of the searching results miss desired position because of local noise. Several inaccurate landmarks will drag the shape from desired position. It is difficult for ASM and OF-ASM to locate points around landmarks near ears and jaw. But we can also learn about that optimal features can model contour appearance more accurately. With the help of optimal features, R-ASM can accurately locate the cheek contour. Searching results of R-ASM are well trapped in a local area. It is clear that R-ASM can improve search results and get a smoother border.

6.2. Experiments on Facial Contour

A total of 96 landmarks are labeled manually on each face image. The PCA thresholds are set to 95% for every ASMs. Five landmarks are inserted into two eyes to present horizontal connected line. And five landmarks are inserted between mouth and horizontal line to present the vertical line. For the sake of simplicity, optimal features don't used in this subsection. The results are shown in table 1. The F.S.O. means five sense organs. Location error, measured in pixel, is average landmarks distance between search results and manually labeled landmarks. It is clear that results of R-ASM are much more accurate than those of ASM especially on cheek contour.

Table 1. Location errors of canonical ASM and R-ASM

	Face	F.S.O	Cheek Contour
ASM	7.74	6.45	11.4
Our algorithm	4.63	4.32	5.36
Improvement	40.2%	33.0%	52.9 %

Fig.4 shows a set of searching results of ASM and R-ASM. In the case, there are wrinkles and shadings on the facial contour or other facial sub-parts. As in Tab.1, ASM couldn't locate the cheek contour very well. It is clear that R-ASM can recover shapes from local noise. A direct reason is that the shape variation is restricted in a local area. The Bayesian inference and RSS hold the whole shape and smooth the border.

7. Conclusion

The purpose of ASM is to learn a smooth object contour from a given input image. Different from other ASM methods that aim to learn a smooth contour in the searching stage, this paper introduces a regularized ASM to impose a natural smooth constrain on ASM's PCA model to learn smooth basis shapes. Bayesian estimation is further discussed to give a coarse-to-fine shape parameter regularization approach. We firstly focus on shape's large variation and then deal with shape's local details. We also introduce an inner shape to give a simple yet robust pose parameter estimation. Comparison results show the effectiveness and efficiency of the proposed method. Our method can easily be extended to other ASM methods.

Acknowledgements

This work was supported by the following funds: Chinese National Natural Science Foundation Project #60518002, Chinese National 863 Program Projects #2006AA01Z192, #2006AA01Z193, and #2006AA780201-4, Chinese National Science and Technology Support Platform Project #2006BAK08B06, and Chinese Academy of Sciences 100 people project, and AuthenMetric R&D Funds.

Appendix

A. Matrix Representation of *E(F)*

Define v_{ic} $=(v_x(1),\ldots, v_x(M),v_y(1),\ldots,v_y(M))$ be a column vector where $c\in\{x,y\}$ and $v_c(i')\in\{0,1\}$ is an indicator function with $v_c(i')=1$ when $i'=i$ or $v_c(i')=0$ otherwise. Now $F_{nx}(i)=F_n^T v_{ix}$, where T is the transpose, and

$$F_{nx}(i)-F_{nx}(i-1)=F_n^T(v_{ix}-v_{ix}) \tag{25}$$

With these $E(F_n)$ of Equ.(11) can be rewritten as follows:

$$F_n^T\sum_i[(v_x(i)-v_x(i-1))(v_x(i)-v_x(i-1))^T+ \tag{26}$$
$$(v_y(i)-v_y(i-1))(v_y(i)-v_y(i-1))^T]F_n$$

Hence

$$E(F_n)=F_n^T V F_n \tag{27}$$

and

$$E(F)=\sum_{n=1}^{N} w_n F_n^T V F \tag{28}$$

However, we notice that there are no data when i=1, something should be modified to tackle this issue. In this context, we use natural boundary conditions and set $F_{nx}(1)=F_{nx}(2)$ and $F_{ny}(1)=F_{ny}(2)$. Therefore, under the natural boundary conditions, we have

$$F_{nx}(i)=\begin{cases}F_n^T(v_{ix}-v_{(i-1)x}), & i\neq 1\\ F_n^T(v_{2x}-v_{1x}), & i=1\end{cases} \tag{29}$$

$$F_{ny}(i)=\begin{cases}F_n^T(v_{iy}-v_{(i-1)y}), & i\neq 1\\ F_n^T(v_{2y}-v_{1y}), & i=1\end{cases} \tag{30}$$

and V defined in Equ.(21) should be accurately written as

$$\begin{aligned}V=&\sum_i\delta(i\neq 1)(v_{ix}-v_{(i-1)x})(v_{ix}-v_{(i-1)x})^T\\ &+\delta(i=1)(v_{2x}-v_{1x})(v_{2x}-v_{1x})^T\\ &\sum_i\delta(i\neq 1)(v_{iy}-v_{(i-1)y})(v_{iy}-v_{(i-1)y})^T\\ &+\delta(i=1)(v_{2y}-v_{1y})(v_{2y}-v_{1y})^T\end{aligned} \tag{31}$$

where δ is a binary function that δ is 1 if the input is true otherwise it is 0. Then we can get Equ. (12).

References

[1] T. F. Cootes, C. J. Taylor, D. Cooper, and J. Graham. Active shape models—Their training and application, Comput. Vis. Image Understanding, vol.61, no.1, (1995.) 38–59.

[2] T.F. Cootes, and C.J.Taylor. Statistical models of appearance for computer vision, Wolfson Image Anal. Unit, Univ. Manchester, Manchester, U.K., Tech. Rep., 1999.

[3] Y. Zhou, L. Gu and H.J. Zhang. Bayesian tangent shape model: Estimating shape and pose parameters via Bayesian inference. In IEEE Conf. on Computer Vision and Pattern Recognition, Madison, WI, June 2003.

[4] J. Coughlan and S. Ferreira. Finding deformable shapes using loopy belief propagation, 2002. In The Seventh European Conference on Computer Vision, Copenhagen, Denmark.

[5] L. Liang, F. Wen, X. Tang, and Y. Xu. An integrated model for accurate shape alignment, 2006. In ECCV, volume IV, pages 333-346, Graz, Austria.

[6] L. Liang, F.Wen, Y.-Q. Xu, X. Tang, and H.-Y. Shum. Accurate face alignment using shape constrained markov network, 2006. CVPR 1313-1319.

[7] Y.Z. Li and W. Ito. Shape parameter optimization for Adaboosted active shape model, ICCV (2005)259- 265

[8] T. Brox, B. Rosenhahn and J. Weickert. Three-Dimensional Shape Knowledge for Joint Image Segmentation and Pose Estimation. Pattern Recognition, LNCS 3663, pp. 109-116, Wien, 2005

[9] B.V. Ginneken, A.F. Frangi, J.J. Staal, B.M. ter Har Romeny, and M.A. Viergever. Active shape model segmentation with optimal features. IEEE Transactions on Medical Imaging, 21(8), (2002) 924–933.

[10] F. Sukno, S. Ordas, C. Butakoff, S. Cruz, and A.F. Frangi. Active shape models with invariant optimal features IOF-ASMs. In Proc. AVBPA, New York, USA, (2005). 365–375.

[11] S. Zhang, L.F. Wu1, Y. Wang, Cascade MR-ASM for Locating Facial Feature Points, The 2nd International Conference on Biometrics, 2007

[12] Y. Huang, Q. Liu, D. Metaxas. A Component Based Deformable Model for Generalized Face Alignment. On Eleventh IEEE International Conference on Computer Vision, 2007

[13] I. Dryden, and K.V. Mardia. The Statistical Analysis of Shape. London,U.K.: Wiley, 1998

[14] C. Goodall, Procrustes methods in the statistical analysis of shapes, J.Roy. Statist. Soc. B, vol. 53, no. 2, pp. 285–339, 1991.

[15] K. Messer, J. Matas, J. Kittler, J. Luettin, and G. Maitre. XM2VTSDB: The extended M2VTS database. In Proc. AVBPA, pages 72–77, 1999.

[16] Hamarneh, G. Active Shape Models with Multi-resolution, http://www.cs.sfu.ca/~hamarneh/software/asm/index.html

[17] P. Viola and M. Jones, Robust Real Time Object Detection. Proc. IEE ICCV Workshop Statistical and Computational Theories of Vision, July 2001

[18] S.Z. Li. Markov Random Field Modeling in Image Analysis. Springer, 2001

[19] Kudo, M. and Sklansky, J. Comparison of algorithms that select features for pattern classiers. Pattern Recognition, 2000, 25–41

[20] V. Blanz, A. Mehl, T. Vetter, H. Seidel. A Statistical Method for Robust 3D Surface Reconstruction from Sparse Data. 3D Data Processing, Visualization and Transmission, 2004